Eur. Phys. J. D **30**, 431–439 (2004)
DOI: 10.1140/epjd/e2004-00106-3

THE EUROPEAN PHYSICAL JOURNAL D

Vacuum Rabi splitting for multilevel electromagnetically induced transparency system

A. Joshi[a] and M. Xiao

Department of Physics, University of Arkansas, Fayetteville AR 72701, USA

Received 12 April 2004 / Received in final form 23 June 2004
Published online 24 August 2004 –

Abstract. We discuss the vacuum Rabi splitting (VRS) from multilevel atoms under electromagnetically induced transparency condition within the framework of linear absorption-dispersion theory. Sharp resonance features superimposed on usually occurring VRS doublet to three-peaked structure spectra are obtained here which can be engineered to have absorptive, dispersive, or dip like profiles according to the choice of system parameters such as radiative damping constants, atomic detunings and driving field strengths etc.

PACS. 42.50.Pq Cavity quantum electrodynamics; micromasers – 42.50.Ar Photon statistics and coherence theory

1 Introduction

Vacuum Rabi splitting (VRS) is considered as one of the important landmarks to achieve non-perturbative regime of cavity quantum-electrodynamics (QED) [1]. VRS has been studied from microwave regime to optical regime and from multi-atomic system to a single atom system. Experiments of cavity QED in non-perturbative or strong coupling regime for single atom were reported in the microwave domain using Rydberg atoms [2–7]. In one of the pioneering work of cavity QED, Haroche et al. [2] experimentally demonstrated self-induced Rabi oscillations in a collection of N Rydberg atoms inside a resonant millimeter-wave cavity. In this experiment the atoms exchanged energy back and forth at a rate $2\wp\varepsilon_0\sqrt{N}/\hbar$ (where $\wp$: dipole matrix element of atomic transition, ε_0: electric field per photon) in the microwave cavity. With the strong coupling regime it is understood that the atom-field coupling constant (g_0) is much larger than the radiative decay rate of atom (γ_a) as well as the rate of cavity damping of field (γ_{cav}). For single atom this implies $g_0 \gg \gamma_a, \gamma_{cav}$ and for N atoms it means that $g_0\sqrt{N} \gg \gamma_a, \gamma_{cav}$. With the developments in cavity QED experiments, the strong coupling regime was obtained in optical domain also. In the optical domain, observations of the VRS for $N \gg 1$ atoms were reported in the experiments by Raizen et al. [8] and Zhu et al. [9]. The number of atoms were brought down to the level of one atom on the average in cesium atomic beam experiment [10] for observing VRS in the optical domain. In another experiment, using rubidium Rydberg atoms in a superconducting niobium microwave cavity, VRS corresponding to $N = 3$ atoms had been observed [6]. The physical origin of VRS can well be explained using the dressed state picture [11]. The name 'vacuum Rabi splitting' suggests a phenomenon associated with quantum mechanics but it has been explained using the classical theory of linear absorption-dispersion [9]. In other words, the VRS is just a normal-mode splitting of coupled harmonic oscillator in which one of the oscillator is single mode field of the cavity and another oscillator is atomic dipole. Very recently, the related effect of Rabi oscillations has got a profound importance in the semiconductor systems of quantum wells, quantum dots, and micro-cavities etc. [12–14].

Discovery of the phenomenon of electromagnetically induced transparency (EIT) in the last decade has given a great deal of impact in the areas of quantum and nonlinear optics by providing control for the speed of light in terms of group velocity modification, lasing without inversion, potential to fabricate efficient electro-optic devices etc. [15]. The EIT is exhibited as a result of quantum interference and the induced atomic coherence in multilevel atomic system is responsible for the modification of linear absorption and dispersion of the atomic-medium [16,17]. The EIT systems also exhibit enhanced non-linear processes, e.g., harmonic generation [18], four-wave mixing [19], two-photon absorption [20], all-optical switching [21], optical multistability [22], slow light [23], and electromagnetically induced focusing [24].

Here we report the VRS spectrum within the frame work of classical model of linear absorption-dispersion for

[a] e-mail: ajoshi@uark.edu

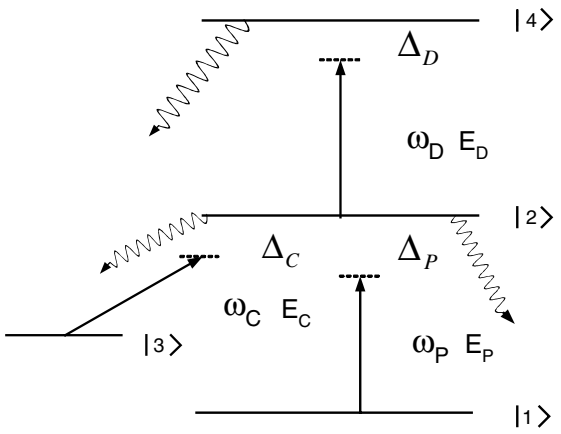

Fig. 1. Schematic diagram of a four-level atomic system in inverted-Y configuration. Here, ω_P, ω_C, and ω_D are frequencies of probe, coupling, and pumping fields, respectively.

a multilevel atomic system contained in a unidirectional optical ring cavity or a Fabry-Perot (FP) cavity where multiple beam interference theory is applied to calculate the cavity transmission function. The multilevel atomic system considered here is a four-level inverted Y-type system which can be reduced to a three-level Λ-type system by taking-off one laser beam. The three-level Λ-type system has been extensively studied both theoretically as well as experimentally as an EIT system useful from a slow light medium to quantum memory medium [25]. Since both linear absorption and dispersion are greatly modified for the EIT system in comparison to their two-level counterparts, so it becomes interesting to analyze how VRS spectrum gets modify for such systems when compared with a two-level system. The remaining part of the manuscript is organized as follows. In Section 2, we present the model for calculating VRS spectrum for the four-level EIT atomic medium inside an optical ring/FP cavity. In Section 3, results are presented for the multi-level EIT systems along with discussions. This is followed by a summary and some concluding remarks in Section 4.

2 The model

The atomic model we use in this work is a closed four-level system in inverted-Y type configuration as shown in Figure 1. This kind of system has been experimentally realized in rubidium atoms. Levels $|1\rangle$, $|2\rangle$, and $|3\rangle$ are in usual three-level Λ-type configuration and level $|4\rangle$ along with levels $|1\rangle$ and $|2\rangle$ forms a three-level ladder-type configuration. So, this composite system is consisting of two three-level sub-systems, viz., a Λ-type and another ladder-type. The transition $|1\rangle$ to $|2\rangle$ (with atomic transition frequency ω_{12}) interacts with a weak probe field (E_P) of frequency ω_P. A coupling field E_C of frequency ω_C drives the transition $|3\rangle$ to $|2\rangle$ (with atomic transition frequency ω_{23}). We have another pumping field E_D of frequency ω_D acting on the transition $|2\rangle$ to $|4\rangle$ (with atomic transition frequency ω_{24}). The radiative damping constants from $|4\rangle$ to $|2\rangle$, $|2\rangle$ to $|3\rangle$, and $|2\rangle$ to $|1\rangle$ being γ_3, γ_2, and γ_1, respectively. The corresponding atomic detunings (Rabi frequencies) for these transitions are $\Delta_D = \omega_{24} - \omega_D$ (Ω_D), $\Delta_C = \omega_{23} - \omega_C$ (Ω_C), and $\Delta_P = \omega_{12} - \omega_P$ (Ω_P), respectively. The non-radiative decay constant of level $|3\rangle$ to level $|1\rangle$ is γ_0. The system becomes a standard Λ-type EIT configuration if there is no pumping field E_D present. Hence we can study both the three-level Λ-type EIT system as well as the 4-level inverted-Y type EIT system using this model.

The density-matrix equation of motion in dipole and rotating-wave approximation for this system can be written down as follows:

$$\begin{aligned}
\dot{\rho_{11}} &= 2\gamma_1\rho_{22} + 2\gamma_0\rho_{33} + i\Omega_P(\rho_{12} - \rho_{21}),\\
\dot{\rho_{22}} &= -2(\gamma_1+\gamma_2)\rho_{22} + 2\gamma_3\rho_{44} - i\Omega_P(\rho_{12} - \rho_{21})\\
&\quad - i\Omega_C(\rho_{32} - \rho_{23}) - i\Omega_D(\rho_{24} - \rho_{42}),\\
\dot{\rho_{33}} &= 2\gamma_2\rho_{22} - 2\gamma_0\rho_{33} + i\Omega_C(\rho_{32} - \rho_{23}),\\
\dot{\rho_{44}} &= -2\gamma_3\rho_{44} + i\Omega_D(\rho_{24} - \rho_{42}),\\
\dot{\rho_{12}} &= -(\gamma_1+\gamma_2 - i\Delta_P)\rho_{12} + i\Omega_C\rho_{13}\\
&\quad + i\Omega_D\rho_{14} + i\Omega_P(\rho_{11} - \rho_{22}),\\
\dot{\rho_{14}} &= -(\gamma_3 - i(\Delta_P + \Delta_C))\rho_{14} + i\Omega_D\rho_{12} - i\Omega_P\rho_{24},\\
\dot{\rho_{24}} &= -(\gamma_1+\gamma_2+\gamma_3 - i\Delta_D)\rho_{24} - i\Omega_P\rho_{14}\\
&\quad - i\Omega_C\rho_{34} + i\Omega_D(\rho_{22} - \rho_{44}),\\
\dot{\rho_{13}} &= -(-i(\Delta_P - \Delta_C) + \gamma_0))\rho_{13} + i\Omega_C\rho_{12} - i\Omega_P\rho_{23},\\
\dot{\rho_{32}} &= -(\gamma_1+\gamma_2 - i\Delta_C)\rho_{32} + i\Omega_P\rho_{31}\\
&\quad + i\Omega_D\rho_{34} + i\Omega_C(\rho_{33} - \rho_{22}),\\
\dot{\rho_{34}} &= -(-i(\Delta_C + \Delta_D) + \gamma_0 + \gamma_3)\rho_{34}\\
&\quad + i\Omega_D\rho_{32} - i\Omega_C\rho_{24},
\end{aligned} \tag{1}$$

with the trace condition $\sum_i \rho_{ii} = 1$.

We confine the above discussed atomic system either as a vapor cell or atoms falling from a MOT (magneto-optic trap) in a unidirectional ring cavity of length L_{cav} with a travelling plane wave (neglecting the transverse effect). The probe transmission frequency is very near to a cavity resonance (transmission peak) of frequency ω_{cav}. The transmission (reflection) coefficient of the cavity mirrors be T(R). The atomic number density of the EIT system be $n = N/V$, where V is the cavity volume. The atomic sample is contained in the length L such that $L < L_{cav}$. By making use of the multiple beam interferometric analysis we get the cavity transmission function as [26]

$$T_C(\omega_P) = \frac{T^2 e^{-\beta L}}{(1 - Re^{-\beta L})^2 + 4Re^{-\beta L}\sin^2(\Phi(\omega_P)/2)}, \tag{2}$$

where βL represents the absorption in a single pass. Note that we obtain the similar expression of $T_C(\omega_P)$ for a FP cavity by adopting plane-wave approximation so that

all transverse effects are neglected [9,27]. The round trip phase shift $\Phi(\omega_P)$ through the cavity is given by

$$\Phi(\omega_P) = (\Delta_P - \Delta_{cav})/\Delta_F + 2(\eta - 1)L\omega_P/c, \quad (3)$$

where the cavity detuning is $\Delta_{cav} = \omega_{cav} - \omega_{12}$, the atomic detuning is $\Delta_P = \omega_P - \omega_{12}$, and the free spectral range of the empty cavity is $\Delta_F = c/2L_{cav}$, with c as the speed of light in vacuum. The empty cavity resonance width is defined as $\gamma_{cav} = \Delta_F/F$, where F is the finesse of cavity given by $F = \pi\sqrt{R}/(1-R)$. The coefficient related to the linear absorption (β) and the linear dispersion (η) for the four-level inverted-Y system under weak probe field excitation is given by

$$\beta \sim \alpha_0 \times \mathrm{Re}\frac{\gamma_1}{(\gamma_1+\gamma_2-i\Delta_P)+\frac{\Omega_C^2}{\gamma_0-i(\Delta_P-\Delta_C)}+\frac{\Omega_D^2}{\gamma_3-i(\Delta_P+\Delta_D)}}, \quad (4)$$

$$\eta \sim 1-\alpha_0 \times \mathrm{Im}\frac{\gamma_1}{(\gamma_1+\gamma_2-i\Delta_P)+\frac{\Omega_C^2}{\gamma_0-i(\Delta_P-\Delta_C)}+\frac{\Omega_D^2}{\gamma_3-i(\Delta_P+\Delta_D)}}, \quad (5)$$

in which $\alpha_0 = 2f_0ne^2/mc\gamma_1$ is defined as the absorption coefficient at the line center, f_0 is the oscillator strength of the transition $|1\rangle$ to $|2\rangle$, and $e(m)$ is electronic charge (mass) parameter.

At this stage we discuss the preparation of EIT system for our study. For this purpose, we consider only the three-level Λ-type system consisting of levels $|1\rangle$, $|2\rangle$ and $|3\rangle$. The EIT effect in this system is due to the atomic coherence ρ_{13} between two ground states which is created by the coupling field. In the dressed state picture, the common excited level $|2\rangle$ can be viewed as two dressed states ($|d_1\rangle$ and $|d_2\rangle$) through the ac Stark-splitting or Autler-Townes effect created by the pumping field and EIT is due to the combination of ac Stark-splitting and interference between these two dressed states. The spontaneous decay processes from the dressed states ($|d_1\rangle$ and $|d_2\rangle$) are not independent random processes and there is a correlation between these two decay processes. So, the Fano interference between absorption path from $|1\rangle$ to $|d_1\rangle$ and from $|1\rangle$ to $|d_2\rangle$ will lead to no-absorption at center frequency from the probe field even Ω_C is much smaller than γ_1 or γ_2. In this work we will consider mainly this regime of Ω_C and Ω_D, i.e., Ω_C, $\Omega_D \ll \gamma_1, \gamma_2$, etc. so that we do not disturb much the two-level atomic system which is being probed by the probe laser. However, we will give some results for relatively larger values of Ω_C/γ_1 and Ω_D/γ_1 also.

3 Results and discussion

3.1 Three-level Λ-type atom

We first study the three-level EIT system in Λ-type configuration of its levels. This can be obtained by setting simply $\Omega_D = 0$ in our general four-level configuration in Figure 1 and the expressions for β and η in this case take the following form

$$\beta \sim \alpha_0 \mathrm{Re}\left[\frac{\gamma_1}{(\gamma_1+\gamma_2-i\Delta_P)+\frac{\Omega_C^2}{\gamma_0-i(\Delta_P-\Delta_C)}}\right], \quad (6)$$

$$\eta \sim 1-\alpha_0 \mathrm{Im}\left[\frac{\gamma_1}{(\gamma_1+\gamma_2-i\Delta_P)+\frac{\Omega_C^2}{\gamma_0-i(\Delta_P-\Delta_C)}}\right]. \quad (7)$$

Substituting equations (6, 7) into equation (2) leads to the desired VRS spectra for the three-level EIT system in Λ-type configuration under various parametric conditions.

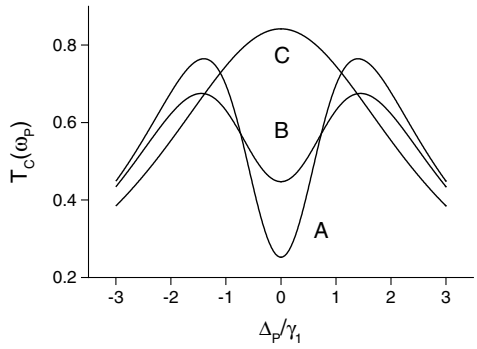

Fig. 2. Cavity transmission function with respect to the normalized probe frequency. The cavity resonance is tuned to the probe transition of the atom ($\Delta_{cav} = 0$), $\Delta_F/\gamma_1 = 750$, $\gamma_{cav}/\gamma_1 = 1.5$, $\alpha_0 L = 0.02$, and $F = 500$. Curves A, B, and C, are for a two-level atom with ($\gamma_1 = 1$, $\gamma_2 = 0$), three-level atom with ($\gamma_1 = 1$, $\gamma_2 = 1$), and three-level atom with ($\gamma_1 = 1$, $\gamma_2 = 10$), respectively.

In Figure 2, we plot VRS spectrum for a two-level atom (curve A). The parameters selected for this purpose are $\alpha_0 L = 0.02$ (low single pass absorption), $\Delta_F/\gamma_1 = 750$ (selecting a high finesse optical cavity), $\gamma_{cav}/\gamma_1 = 1.5$ (almost equal cavity and atomic resonance widths), and $\Delta_{cav} = 0$ (assuming atom-cavity resonance condition). The curve B in Figure 2 represents the effect of second nearby ground level with decay constant $\gamma_2/\gamma_1 = 1.0$ (but without any field, i.e., $E_C = 0$). Clearly, both the peaks become broader but still resolvable. In curve C (Fig. 2) we keep $\gamma_2/\gamma_1 = 10.0$ ($E_C = 0$) and the two peaks merged into a single peak. In the presence of nearby ground level ($E_C = 0$) the system behaves like an effective two-level atomic system having two decay channels from the excited state. The behavior of the system, meaning VRS gets resolved into two peaks is governed by the larger γ_i, ($i = 1, 2$) value relative to FSR [8]. As we are keeping $\alpha_0 L$ and γ_1 unchanged and only varying γ_2/γ_1, so it is clear from equation (2) that the cavity transmission peaks as a function of Δ_P/γ_1 are getting broader in width and reducing in height with increase in γ_2/γ_1 value till they merge and become a single peak but then the height increases.

Also, the slope of the function $\Phi(\omega_P)$ provides qualitative idea about the width of cavity transmission profile. It is easy to verify that the slope of $\Phi(\omega_P)$ decreases around

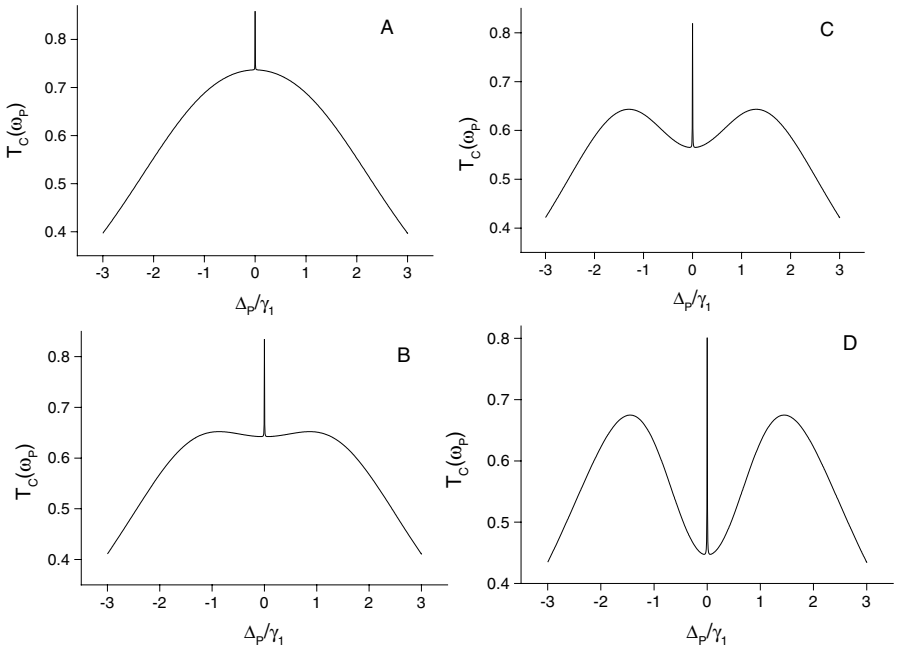

Fig. 3. Cavity transmission function with respect to the normalized probe frequency for a three-level EIT system in Λ configuration with $\Omega_C/\gamma_1 = 0.08$, $\gamma_0/\gamma_1 = 10^{-3}$, and other parameters same as in Figure 2. Curve A B, C, and D are for $\gamma_2/\gamma_1 = 5$, 3, 2, and 1, respectively.

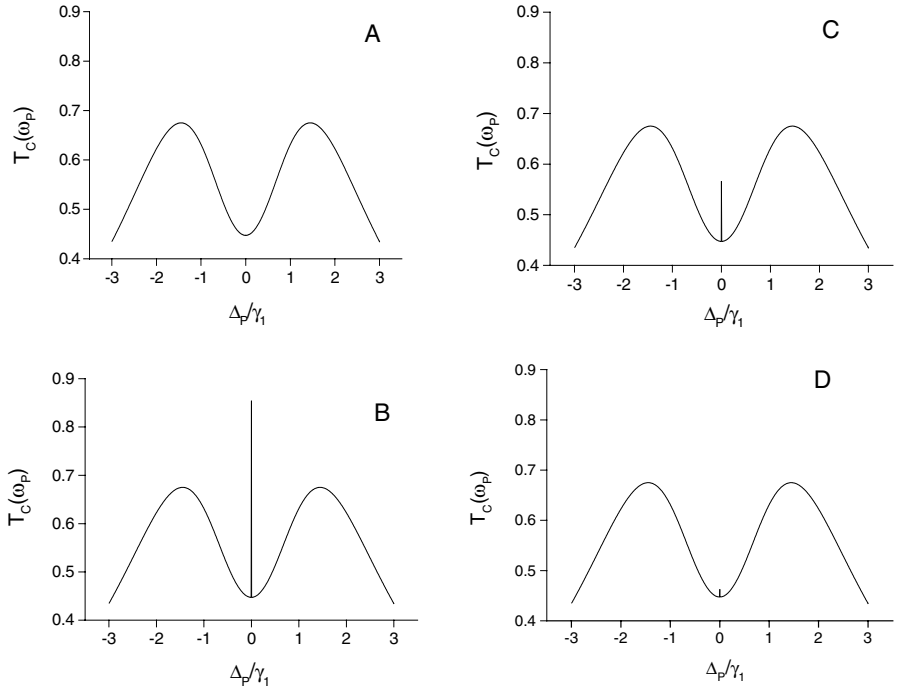

Fig. 4. Cavity transmission function with respect to the normalized probe frequency for a three-level EIT system in Λ configuration with $\Omega_C/\gamma_1 = 0.01$, $\gamma_2/\gamma_1 = 1.0$, and other parameters same as in Figure 2. Curve A is for an effective two-level atom ($\Omega_C = 0$, $\gamma_0/\gamma_1 = 0$) but curves B, C, and D are for the three-level system with $\gamma_0/\gamma_1 = 10^{-5}, 10^{-4}$, and 10^{-3}, respectively.

$\Delta_P = 0$ with increase in γ_2/γ_1, causing broadening of cavity transmission resonances, such that they can not be resolved when $\gamma_2/\gamma_1 = 10$ (curve C, Fig. 2) under the FSR selected in this case. The zeros of $\Phi(\omega_P)$ provides the number of peaks (having absorption profile like features) in VRS spectrum. If $\Phi(\omega_P)$ has one zero then there is only one transmission peak. For three zeros there are two peaks in VRS spectrum, for five zeros there are three peaks in VRS spectrum and so on. The slopes of $\Phi(\omega_P)$ at these zeros provide the widths of the resonances as discussed above.

Next, we discuss the VRS spectrum in a true Λ-type EIT system (shown in Fig. 3) with $\Omega_C/\gamma_1 = 0.08$, $\gamma_0/\gamma_1 = 10^{-3}$, $\Delta_C/\gamma_1 = \Delta_D/\gamma_1 = 0$, $\Omega_D/\gamma_1 = 0$ and remaining parameters same as in Figure 2. Curves A, B, C, and D are for $\gamma_2/\gamma_1 = 5$, 3, 2, and 1, respectively. It is clear from Figure 3 that VRS spectrum changes for EIT system in comparison to the two-level system. We get a sharp cavity transmission resonance at $\Delta_P/\gamma_1 = 0$ besides one or two broad transmission peaks depending on the value of γ_2/γ_1 as discussed above (Fig. 2). In Figure 4, we study the effect of γ_0/γ_1 on the VRS spectrum of the

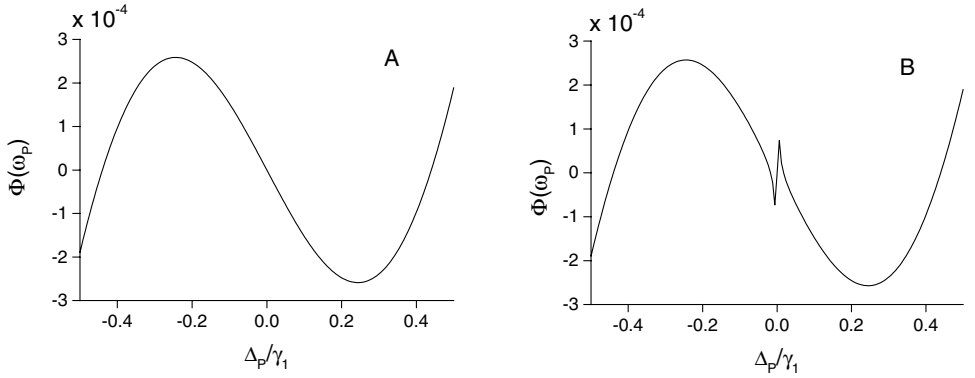

Fig. 5. The round trip phase-shift experienced by the field in the cavity. Curves A and B are for the parametric conditions of Figures 4A and 4B, respectively.

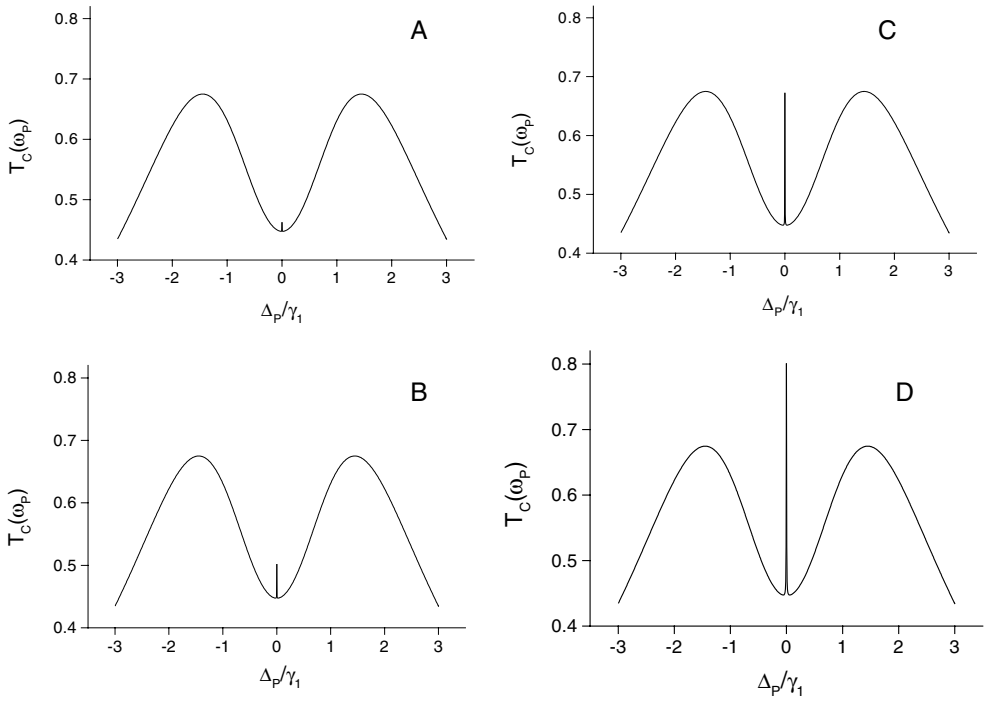

Fig. 6. Cavity transmission function with respect to the normalized probe frequency for a three-level EIT system in Λ configuration with $\Delta_C/\gamma_1 = 0.0$, $\gamma_2/\gamma_1 = 1.0$, $\gamma_0/\gamma_1 = 10^{-3}$, and other parameters same as in Figure 2. Curves A, B, C, and D are for $\Omega_C/\gamma_1 = 0.01, 0.03, 0.05,$ and 0.08, respectively.

EIT system with $\Omega_C/\gamma_1 = 0.01$, $\gamma_2/\gamma_1 = 1$, and other parameters same as in Figure 2. Curve A, which is for the effective two-level system with $\gamma_2/\gamma_1 = 1$, $\Omega_C = 0$, is given here just for the sake of comparison. Curves B, C, and D are for $\gamma_0/\gamma_1 = 10^{-5}, 10^{-4}$, and 10^{-3}, respectively. By keeping $\Omega_C/\gamma_1 \ll 1$, we are more or less maintaining the undisturbed two-level atom condition for the probe transition. The sharp resonance peak is a sensitive function of γ_0/γ_1. As γ_0/γ_1 increases this central sharp peak in VRS spectrum diminishes in amplitude (curves B to D). We have depicted $\Phi(\omega_P)$ in Figures 5A and 5B for the two cases discussed above in Figures 4A and 4B. Clearly, $\Phi(\omega_P)$ crosses three times the x-axis in Figure 5A and have two peaks in the VRS spectrum while it crosses x-axis five times in Figure 5B and hence have three peaks in the VRS spectrum. The slope of $\Phi(\omega_P)$ around $\Delta_P = 0$ is very steep in Figure 5B and hence the width of this peak is very small (a sharp resonance) in Figure 4B.

Figure 6 displays the effect of increasing coupling field strength on the VRS spectrum of the three-level Λ-type EIT system. For this purpose we keep $\gamma_2/\gamma_1 = 1.0$, $\gamma_0/\gamma_1 = 10^{-3}$, $\Delta_C/\gamma_1 = 0$ and the remaining parameters same as in Figure 2. Curves A, B, C, and D are for $\Omega_C/\gamma_1 = 0.01, 0.03, 0.05$, and 0.08, respectively. The sharp central cavity transmission resonance situated at $\Delta_P/\gamma_1 = 0$ becomes more and more prominent in intensity with the increase in coupling field strength (E_C) alone. Physically, this is because the dip in absorption spectrum of EIT system gets enhanced as E_C increases (the increased E_C causes quantum interference to become more prominent). The effect of changing coupling field frequency detuning (Δ_C/γ_1) is presented in Figure 7. The parametric conditions are similar to Figure 6, i.e., we keep $\gamma_2/\gamma_1 = 1.0$, $\gamma_0/\gamma_1 = 10^{-3}$, and $\Omega_C/\gamma_1 = 0.08$ etc. Here curves A, B, C, and D are for $\Delta_C/\gamma_1 = 0.0, 0.5, 1.5,$ and 2.0 respectively. Clearly, the sharp cavity transmission resonance changes its height, shape and direction with the changing value of Δ_C/γ_1. In curve A, this resonance is situated at $\Delta_P/\gamma_1 = 0$ with a normal absorption profile like feature. It changes to dispersion profile like features in curves B and C but with the decrease in magnitude, located at $\Delta_P/\gamma_1 = 0.5$ and 1.0, respectively. Physically,

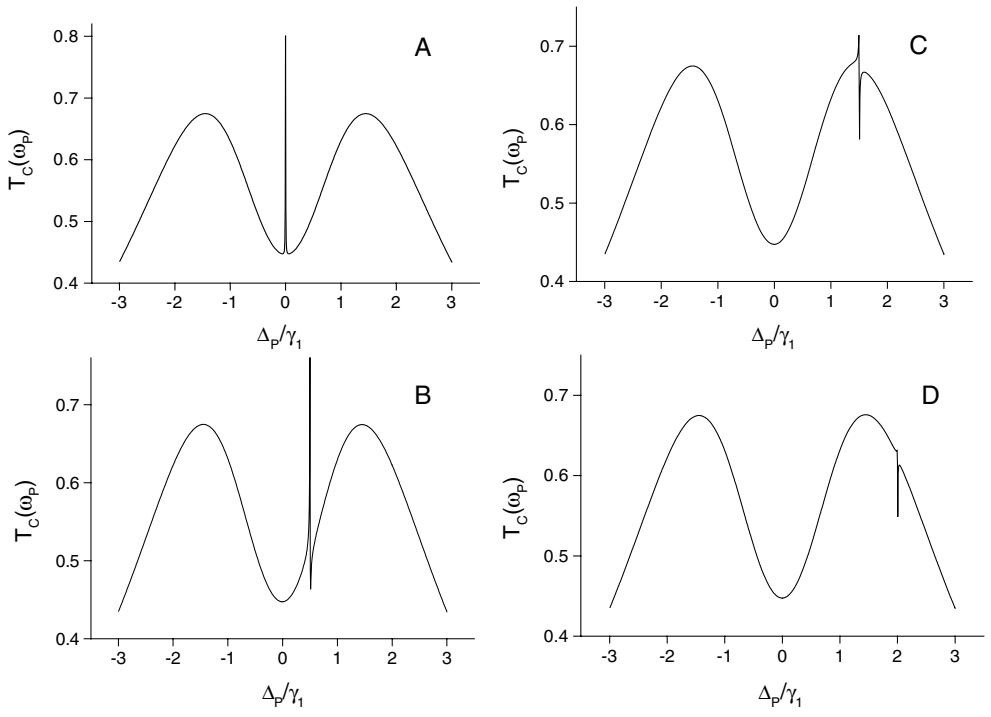

Fig. 7. Cavity transmission function with respect to the normalized probe frequency for a three-level EIT system in Λ configuration with $\gamma_2/\gamma_1 = 1.0$, $\gamma_0/\gamma_1 = 10^{-3}$, $\Omega_C/\gamma_1 = 0.08$, and other parameters same as in Figure 2. Curves A, B, C, and D are for $\Delta_C/\gamma_1 = 0.0, 0.5, 1.5$, and 2.0, respectively.

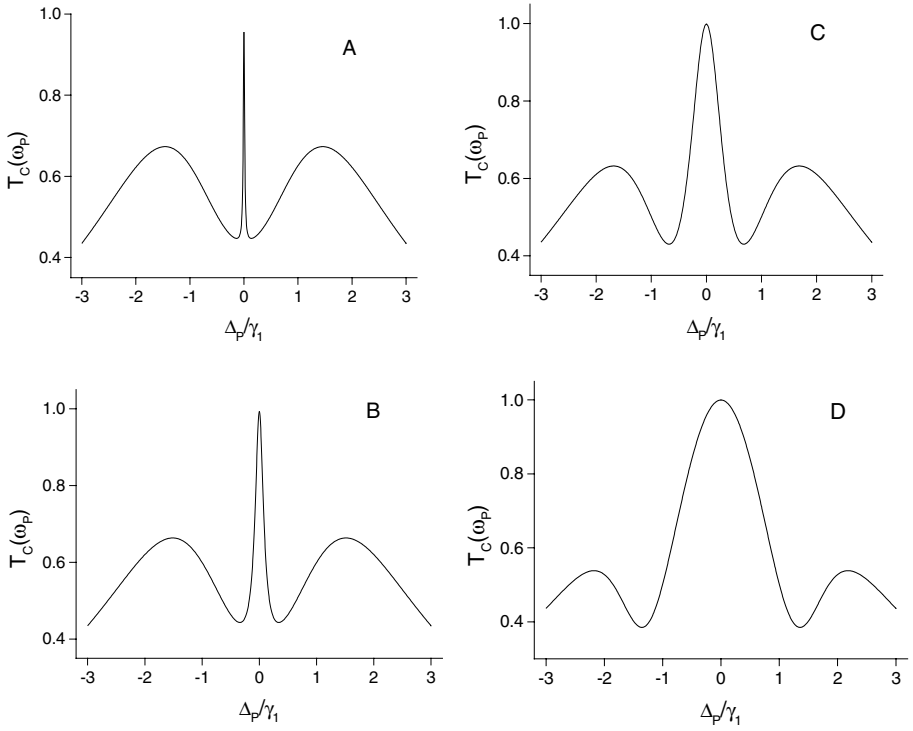

Fig. 8. Cavity transmission function with respect to the normalized probe frequency for a three-level EIT system in Λ configuration with $\gamma_2/\gamma_1 = 1.0$, $\gamma_0/\gamma_1 = 10^{-3}$, $\Delta_C/\gamma_1 = 0.0$, and other parameters same as in Figure 2. Curves A, B, C, and D are for $\Omega_C/\gamma_1 = 0.2$, 0.5, 1.0, and 2.0, respectively.

the characteristics features of three-level Λ-type EIT system under non-zero value of Δ_C/γ_1 are reflected here. Finally at $\Delta_C/\gamma_1 = 2.0$, this transmission peak becomes inverted (a dip) and its location is at $\Delta_P/\gamma_1 = 2.0$. So, it is possible to generate a variety of shape controllable sharp cavity transmission profiles (at desired locations) in the VRS spectrum of an EIT system with the variation of system parameters. Lastly, for this system we consider the effect of higher coupling field strength (E_C) on the VRS spectrum (Fig. 8). In Figure 8, we keep $\gamma_0/\gamma_1 = 10^{-3}$, $\gamma_2/\gamma_1 = 1.0$, $\Delta_C/\gamma_1 = 0$, and remaining all other parameters same as in Figure 2. Curves A, B, C, and D are for $\Omega_C/\gamma_1 = 0.2$, 0.5, 1.0, and 2.0, respectively. For moderately high coupling fields (curves A, B) only the central transmission peak is affected in its width but the side peaks are more or less unchanged. As the coupling field

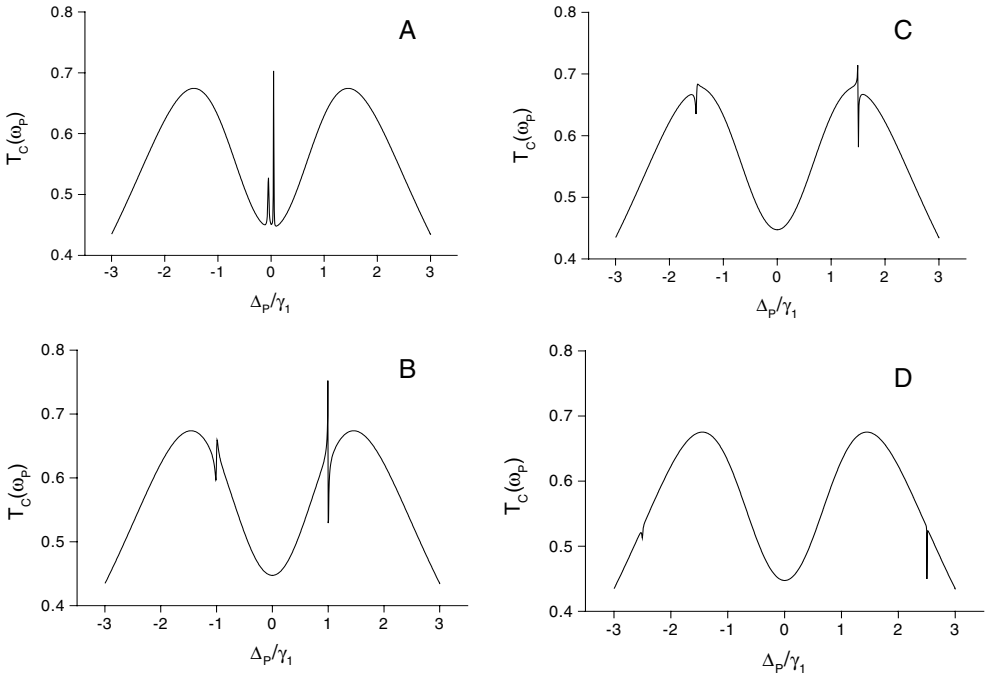

Fig. 9. Cavity transmission function with respect to the normalized probe frequency for a four-level EIT system in inverted-Y configuration with $\gamma_2/\gamma_1 = 1.0$, $\gamma_3/\gamma_1 = 10^{-2}$, $\gamma_0/\gamma_1 = 10^{-3}$, $\Omega_C/\gamma_1 = 0.08$, $\Omega_D/\gamma_1 = 0.08$, and other parameters same as in Figure 2. Curves A, B, C, and D are for $(\Delta_C/\gamma_1, \Delta_D/\gamma_1) = (0.1, 0.1)$, $(1.0, 1.0)$, $(1.5, 1.5)$, and $(2.5, 2.5)$, respectively.

strength is further increased (curves C, D) the width of central peak is further enhanced. Physically, this could be attributed to the widened EIT window as well as prominent Stark effect as a result of enhanced coupling field strength. The magnitudes of the side peaks and their widths also change as the linear absorption-dispersion of the system is greatly modified at higher coupling field strengths.

3.2 Four-level inverted Y-system

The four-level inverted-Y system under consideration is a generalization of the two three-level EIT sub-systems joined together. One of the sub-system is a Λ-type three-level system while the other one is a ladder-type three-level system as discussed above. These two sub-systems cooperate each other in enhancing the EIT phenomenon. Thus one can get here enhanced VRS features over the above discussed Λ-type system for an appropriate choice of the parameters. However, we will discuss only some other interesting observations in VRS spectrum from this system arising under different values of the frequency detuning parameters Δ_C/γ_1 and Δ_D/γ_1. We plot VRS spectrum in Figure 9 with $\gamma_2/\gamma_1 = 1.0$, $\gamma_0/\gamma_1 = 10^{-3}$, $\gamma_3/\gamma_1 = 10^{-2}$, $\Omega_C/\gamma_1 = 0.08$, $\Omega_D/\gamma_1 = 0.08$, and remaining parameters same as in Figure 2. Curves A, B, C, and D are for ($\Delta_C/\gamma_1 = 0.1$, $\Delta_D/\gamma_1 = 0.1$), ($\Delta_C/\gamma_1 = 1.0$, $\Delta_D/\gamma_1 = 1.0$), ($\Delta_C/\gamma_1 = 1.5$, $\Delta_D/\gamma_1 = 1.5$), and ($\Delta_C/\gamma_1 = 2.5$, $\Delta_D/\gamma_1 = 2.5$), respectively. Since the four-level inverted-Y system is a double EIT system so we get two sharp cavity transmission resonances (curve A, Fig. 9) situated at $\Delta_P/\gamma_1 = 0.1$ and -0.1, respectively. Hence, the main characteristics of this kind of EIT system is that now there are four-peaks in the cavity transmission spectrum. Two broader peaks are due to the usual two-level VRS and remaining sharp (with sub-natural linewidths) peaks are because of the double EIT system. With the variation of the values of Δ_C/γ_1 and Δ_D/γ_1, we can alter the relative separation of these sharp peaks, their shapes (absorption profile like feature to dispersion profile like feature or dip like feature), and relative magnitudes etc. which can clearly be seen in curves B, C, and D of Figure 9. The difference in the magnitudes of two sharp peaks in curve A is because the value of γ_3/γ_1 is different from γ_0/γ_1. In order to see the variation of function $\Phi(\omega_P)$ in the four-level inverted-Y system we have plotted this function with respect to Δ_P/γ_1 in Figures 10A and 10B for the two cases discussed above in Figures 9A and 9B. In Figure 10A we find that the function $\Phi(\omega_P)$ is crossing x-axis seven times resulting into four peaks (having absorption profile like features) and the places where variation of its slope is very fast give rise to the sharp features in the cavity transmission spectrum (Fig. 9A). On the contrary, in Figure 10B, we observe one absorption profile like feature and one dip like feature and these correspond to sharp dispersion like features in the cavity transmission spectrum (VRS spectrum, Fig. 9B) of this EIT system. If we reverse the sign of one of the detunigs then both the sharp peaks will be situated on same side and they may coincide with each other if the magnitudes of the two detunings are exactly equal. Thus, we can engineer various patterns on the VRS spectrum by variation of Δ_C/γ_1 and Δ_D/γ_1. Physically, it is because of the characteristics EIT features of the four-level inverted-Y system which influence the VRS spectrum. Finally, in Figure 11 we show the effect of higher coupling and driving field strengths on the VRS spectrum of inverted-Y system. The parameters used for this purpose are $\gamma_0/\gamma_1 = 10^{-3}$, $\gamma_2/\gamma_1 = 1.0$, $\gamma_3/\gamma_1 = 10^{-2}$, $\Delta_C/\gamma_1 = 0.1$, $\Delta_D/\gamma_1 = 0.1$, and remaining parameters same as in Figure 2. In Figure 11, curves A, B,

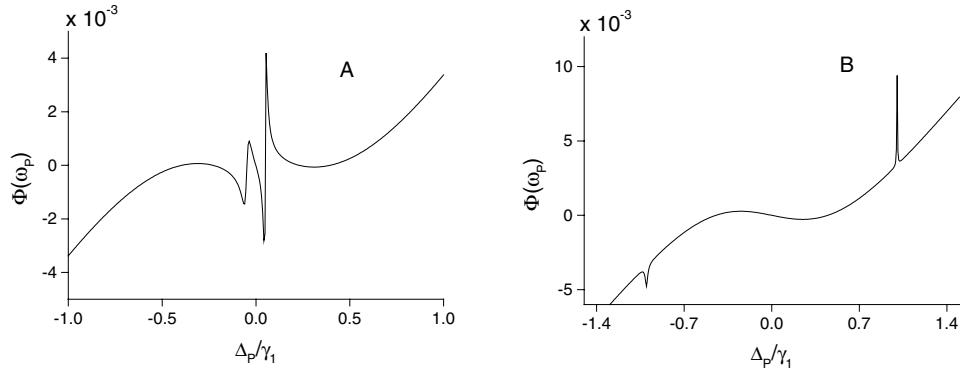

Fig. 10. The round trip phase-shift experienced by the field in the cavity. Curves A and B are for the parametric conditions of Figures 9A and 9B, respectively.

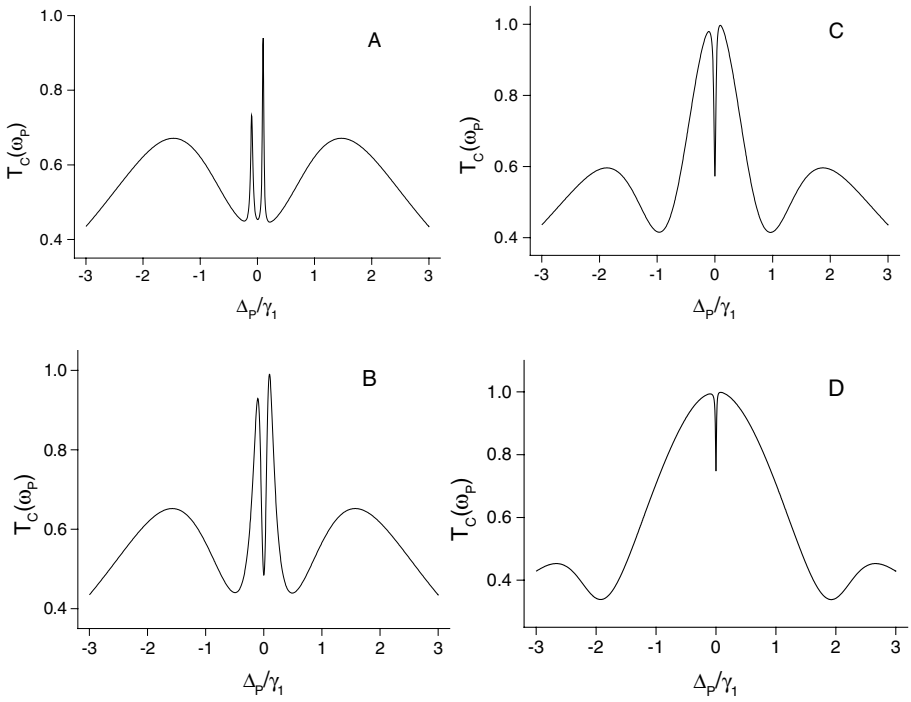

Fig. 11. Cavity transmission function with respect to the normalized probe frequency for a four-level EIT system in inverted-Y configuration with $\gamma_2/\gamma_1 = 1.0$, $\gamma_3/\gamma_1 = 10^{-2}$, $\gamma_0/\gamma_1 = 10^{-3}$, $\Delta_C/\gamma_1 = 0.1$, $\Delta_D/\gamma_1 = 0.1$, and other parameters same as in Figure 2. Curves A, B, C, and D are for $(\Omega_C/\gamma_1, \Omega_D/\gamma_1) = (0.2, 0.2)$, $(0.5, 0.5)$, $(1.0, 1.0)$, and $(2.0, 2.0)$, respectively.

C, and D are for $(\Omega_C/\gamma_1, \Omega_D/\gamma_1) = (0.2, 0.2)$, $(0.5, 0.5)$, $(1.0, 1.0)$, and $(2.0, 2.0)$, respectively. For moderately high field strengths of coupling and driving fields (curves A, B) only the two central peaks are affected in their widths and the remaining two side peaks are more or less unchanged. As we increase the coupling and driving field strengths further, the two central peaks becomes broader and broader and merge together to produce sharp narrow dip in the center (Figs. 11C and 11D). For very high fields just one peak at the center is surviving. This is due to the enhancement of EIT windows as well as Stark effect in both the sub-systems. In curves C and D, magnitudes and widths of the side peaks also change due to the modification in the linear absorption-dispersion characteristic of the system at higher strengths of coupling and driving fields.

4 Summary and conclusions

To summarize, we have studied the vacuum Rabi-splitting from a three-level system in Λ configuration (exhibiting EIT) and a four-level system in inverted-Y configuration (exhibiting double EIT) within the framework of linear absorption-dispersion theory and multiple beam interference analysis of an optical ring resonator. The results are compared with the VRS spectrum of usual two-level atom within the same framework of the analysis. Sharp features (having sub-natural linewidths) in the transmission spectra are obtained because of the EIT exhibited by these systems. The width, height, shape and direction of these sharp features are easily controllable with the system parameters like field strengths, frequency detuning and radiative damping constants. We also get prominent three peaked VRS spectrum when the coupling or/and pumping field strengths are increased. These results are in contrast with the results from a two-level atom. A possible experimental observation of the features predicted in this paper can be realized in a scheme involving hyperfine levels of ^{87}Rb atoms. In this scheme, the levels $|1\rangle$, $|3\rangle$, $|2\rangle$, and $|4\rangle$ being the states $5^2S_{1/2}(F = 1)$, $5^2S_{1/2}(F = 2)$, $5^2P_{1/2}(F' = 1)$ and $5^2D_{3/2}(F'' = 2)$, respectively. The radiative decay constants of levels $|4\rangle$ and $|2\rangle$ are 0.69 MHz

($\sim$ 230 ns) and 5.3 MHz ($\sim$ 30 ns), respectively. The transition dipole moment for the coupling field transition (level $|3\rangle$ to $|2\rangle$) is about 1.5×10^{-29} coulomb meter and for the pumping field transition (level $|2\rangle$ to $|4\rangle$) is 0.2×10^{-29} coulomb meter approximately. The laser power (for coupling and pumping lasers) requirements for the Rabi frequencies used in the above calculation could be in the range from a few microwatt/cm^2 to a few milliwatt/cm^2 for the laser beam spot of size 750 μm. The power requirement for the probe transition is calculated by assuming the intracavity intensity for this transition should be far below from the saturation intensity (which is about 1.7 mW/cm^2 for the probe transition). One can use probe power in a range of a few picowatts/cm^2 for a 80 μm spot size of the laser beam. In a recent proposal a controlled transfer of the quantum state of a photon wavepacket to and from a collective atomic spin excitation using EIT has been shown [25]. Our this work may be useful in cavity quantum electrodynamics implementation of such experiments with more flexibility due to controlled double-EIT for information storage and processing with a very low photon numbers. Also, the time domain analysis related to self-induced Rabi oscillation of these EIT systems on the lines of reference [2] could give very interesting results which will be presented elsewhere.

We acknowledge the funding supports from the National Science Foundation and the Office of Naval Research.

References

1. J.J. Sanchez-Mondragon, N.B. Narozhny, J.H. Eberly, Phys. Rev. Lett. **51**, 550 (1983)
2. Y. Kaluzny, P. Goy, M. Gross, J.M. Raimond, S. Haroche, Phys. Rev. Lett. **51**, 1175 (1983)
3. D. Meschede, H. Walther, G. Muller, Phys. Rev. Lett. **54**, 551 (1985)
4. G. Rempe, H. Walther, N. Klein, Phys. Rev. Lett. **58**, 353 (1987); G. Rempe, F. Schmidt-Kaler, H. Walther, Phys. Rev. Lett. **64**, 2783 (1990)
5. M. Brune, J.M. Raimond, P. Goy, L. Davidovich, S. Haroche, Phys. Rev. Lett. **59**, 1899 (1987)
6. F. Bernardot, P. Nussenzveig, M. Brune, J.M. Raimond, S. Haroche, Europhys. Lett. **17**, 33 (1991)
7. *Cavity Quantum Electrodynamics*, Advances in Atomic, Molcular and Optical Physics, edited by P.R. Berman (Academic, NY, 1994), suppl. 2
8. M.G. Raizen, R.J. Thompson, R.J. Brecha, H.J. Kimble, H.J. Carmichael, Phys. Rev. Lett. **63**, 240 (1989)
9. Y. Zhu, D.J. Gauthier, S.E. Morin, Q. Wu, H.J. Carmichael, T.W. Mossberg, Phys. Rev. Lett. **64**, 2499 (1990)
10. R.J. Thompson, G. Rempe, H.J. Kimble, Phys. Rev. Lett. **68**, 1132 (1992)
11. G.S. Agarwal, Phys. Rev. Lett. **53**, 1732 (1984); J. Opt. Soc. Am. B **2**, 480 (1985)
12. R. Binder, M. Lindberg, Phys. Rev. B **61**, 2830 (2000)
13. T.H. Stievater, X. Li, D.G. Steel, D. Gammon, D.S. Katzer, D. Park, C. Piermarocchi, L.J. Sham, Phys. Rev. Lett. **87**, 133603 (2001)
14. L.C. Andreani, G. Panzarini, J.-M. Gérard, Phys. Rev. B **60**, 13276 (1999); C.M. Savage, H.J. Carmichael, D.F. Walls, Opt. Comm. **42**, 211 (1982)
15. For review, see E. Arimondo, in *Progress in Optics*, edited by E. Wolf (North-Holland, Amsterdam, 1996), Vol. 35; S.E. Harris, Phys. Today **50**(7), 36 (1997); M. Xiao et al., Opt. Photo. News **13**(9), 44 (2002) and references therein; M. Xiao, IEEE J. STQE **9**, 86 (2003)
16. K.J. Boller, A. Imamoglu, S.E. Harris, Phys. Rev. Lett. **66**, 2593 (1991); J.E. Field, K.H. Hahn, S.E. Harris, Phys. Rev. Lett. **67**, 3062 (1991)
17. Y. Li, M. Xiao, Phys. Rev. A **51**, R2703, 4959 (1995); J. Gea-Banacloche, Y. Li, S. Jin, M. Xiao, Phys. Rev. A **51**, 576 (1995); M. Xiao, Y. Li, S. Jin, J. Gea-Banacloche, Phys. Rev. Lett. **74**, 666 (1995); A. Joshi, M. Xiao, Phys. Lett. A **317**, 370 (2003)
18. K. Hakuta, L. Marmet, B.P. Stoicheff, Phys. Rev. Lett. **66**, 596 (1991); A.J. Merriam et al., Phys. Rev. Lett. **84**, 5308 (2000); M. Jain et al., Phys. Rev. Lett. **77**, 4326 (1996)
19. P.R. Hemmer et al., Opt. Lett. **20**, 982 (1995); Y. Li, M. Xiao, Opt. Lett. **21**, 1064 (1996); B. Lu, W.H. Burkett, M. Xiao, Opt. Lett. **23**, 804 (1998)
20. M. Yan, E.G. Rickey, Y. Zhu, Opt. Lett. **26**, 548 (2001)
21. H. Wang, D. Goorskey, M. Xiao, Phys. Rev. A **65**, 051802(R) (2002); A. Brown, A. Joshi, M. Xiao, Appl. Phys. Lett. **83**, 1301 (2003)
22. A. Joshi, M. Xiao, Phys. Rev. Lett. **91**, 143904 (2003); A. Joshi et al., Phys. Lett. A **315**, 203 (2003); A. Joshi et al., Phys. Rev. A **68**, 015806 (2003)
23. L.V. Hau, S.E. Harris, Z. Dutton, C.H. Behroozi, Nature **397**, 594 (1999); M.M. Kash et al., Phys. Rev. Lett. **82**, 5229 (1999)
24. R.R. Moseley, S. Shepherd, D.J. Fulton, B.D. Sinclair, M.H. Dunn, Phys. Rev. Lett. **74**, 670 (1995)
25. M. Fleischhauer, M.D. Lukin, Phys. Rev. Lett. **84**, 5094 (2000); M. Bajcsy, A.S. Zibrov, M.D. Lukin, Nature **426**, 638 (2003)
26. L.A. Lugiato, Theory of Optical bistability in *Progress in Optics*, edited by E. Wolf (North-Holland, Amsterdam, 1984), Vol. 21, p. 71
27. W.E. Schulz, W.R. Macgillivray, M.C. Standage, Phys. Rev. A **36**, 1316 (1987)